SODIUM MAGNETIC RESONANCE IMAGING FOR EVALUATION OF DUCHENNE MUSCULAR DYSTROPHY

An Undergraduate Research Scholars Thesis

by

EDITH VALLE

Submitted to the Undergraduate Research Scholars program at
Texas A&M University
in partial fulfillment of the requirements for the designation as an

UNDERGRADUATE RESEARCH SCHOLAR

Approved by Research Advisor: Dr. Mary P. McDougall

May 2019

Major: Biomedical Engineering

TABLE OF CONTENTS

ABSTRACT

Sodium Magnetic Resonance Imaging for Evaluation of Duchenne Muscular Dystrophy

Edith Valle
Department of Biomedical Engineering
Texas A&M University

Research Advisor: Dr. Mary P. McDougall
Department of Biomedical Engineering
Texas A&M University

Duchenne Muscular Dystrophy (DMD) is a genetic disorder caused by lack of dystrophin, and is characterized by progressive muscle degeneration and weakness. Preliminary magnetic resonance image (MRI) studies have reported that increased tissue sodium concentration (TSC) levels may play a role in the progression of the disease. However, the number of studies reporting this finding are limited. In part, this is due to the fact that ^{23}Na MRI requires the use of customized hardware, pulse sequences and reconstruction techniques. Nonetheless, evaluating abnormal TSC levels may provide valuable information pertaining to disease progression and/or treatment efficacy. To address this need, a custom double-tuned birdcage coil was designed and constructed to evaluate ^{23}Na concentration levels in muscle tissue phantoms using MRI. The coil was constructed with an outer high-pass coil configuration for ^{1}H (200.07 MHz) and an inner low-pass coil configuration for ^{23}Na (52.93 MHz) for a 4.7 T scanner. Bench measurements were taken to evaluate the performance of the coil at both resonant frequencies. The isolation between channels was found to be -25 dB at the ^{1}H frequency and -30.9 dB at the ^{23}Na frequency. The loaded and unloaded quality factors of the coil were evaluated using a phantom that mimicked the loading properties of diseased tissue. The loaded

and unloaded quality factors of ^{1}H were 351.1 and 359.9, respectively. The loaded and unloaded quality factors of ^{23}Na were 293.9 and 300.7, respectively. The B_1 fields were found to be homogeneous in the operating regions of the coils. Finally, preliminary phantom sodium imaging indicated the ability to distinguish between healthy and diseased ^{23}Na concentration levels.

DEDICATION

I dedicate this work to my parents and sister. I owe a life of learning experiences, love and moral support to my family. They have always inspired me to be curious and to believe in myself. Their sacrifices, continuous encouragement and hard work have made it possible for me to be where I am today.

ACKNOWLEDGEMENTS

I would like to first thank my thesis advisor, Dr. Mary McDougall, for her support and guidance throughout this process. My participation in this project would have not been possible without the opportunity she gave me to join her research lab.

I would also like to extend my gratitude to Romina Del Bosque for allowing me to do this project in collaboration with her. Her input and advice have taught me a great deal about research and engineering.

I would also like to thank Matthew Wilcox and Travis Carrell, Dr. McDougall's doctoral students, for the learning opportunities they have provided; as well as their support and patience.

Finally, I would like to thank my parents and siblings for all their support throughout my entire academic career.

NOMENCLATURE

B_1	Radio Frequency Magnetic Field
DMD	Duchenne Muscular Dystrophy
GRMD	Golden Retrievers with Muscular Dystrophy
MRI	Magnetic Resonance Imaging
NMR	Nuclear Magnetic Resonance
Q	Quality Factor
RF	Radio Frequency
SNR	Signal to Noise Ratio
T	Tesla
TIPS	Texas A&M Institute for Preclinical Studies
TSC	Tissue Sodium Concentration

CHAPTER I

INTRODUCTION

Duchenne Muscular Dystrophy (DMD) is a genetic disorder characterized by the absence of the protein dystrophin. This protein is a vital part of the muscle's cytoskeleton; therefore, its absence leads to muscular atrophy. As the disease progresses, respiratory and cardiac muscle become compromised resulting in death in early adulthood (1,2). It has been reported that the absence of dystrophin also has a negative impact on the ability of the voltage-gated sodium channel, $Na_v1.4$, to regulate TSC levels in skeletal muscle. As a result, there is persistent myoplasmic edema, which showed a correlation with cell death in mdx mice (3). Magnetic resonance imaging has been used to study DMD and its progression. However, there are limited studies that evaluate the role sodium plays in the progression of DMD in humans. Studies using substantially equivalent animal models have been performed to examine the disease and the treatment efficacy. It has been reported that golden retrievers with muscular dystrophy (GRMD) closely resemble the development of the disease in humans (1,4,5). For this reason, studying the presence of elevated sodium levels in GRMD models could provide relevant information regarding treatment in humans.

Magnetic resonance imaging utilizes magnetic fields to acquire images and/or spectroscopy of NMR-active nuclei within the body. These images and/or spectroscopy can be acquired with radiofrequency coils tuned to a certain frequency depending on the gyromagnetic ratio of the NMR-active nuclei and the magnetic field strength (6). For this project, a double-tuned birdcage coil was designed and constructed to evaluate muscle tissue phantoms which mimic sodium concentrations of both diseased and healthy muscle tissue. This coil design was

chosen due to its ability to produce a highly uniform magnetic field throughout the entire region of interest. The coil interfaced with a 4.7T Varian Inova scanner. The novelty of this design lies in the application of a custom coil for the study of sodium concentrations similar to those present in DMD patients. Additionally, the contribution to the field lies in enabling the first-time evaluation of the total sodium concentration as a biomarker in the canine model of Duchenne Muscular Dystrophy.

This project is part of a doctoral research project by Romina Del Bosque, a Ph.D. student in the Nuclear Magnetic Resonance Radiofrequency Laboratory at Texas A&M University. The sodium birdcage coil constructed as part of this study will be used in Del Bosque's research project to assess harvested tissue from GRMD models at various stages of treatment.

CHAPTER II

MATERIALS AND METHODS

Birdcage coil design and construction

The design of the linear four-ring double-tuned birdcage coil was customized to the length and diameter of the phantom to maximize signal-to-noise ratio (SNR). The coil consisted of two sets of nested rings with the outer rings and eight rungs between the inner and outer rings corresponding to the ^{1}H frequency and the two inner rings and sixteen rungs between them corresponding to the ^{23}Na frequency, as shown in Figure 1.

Figure 1. Birdcage coil end rings and rungs design.

The rung conductors were etched onto flexible FR4 copper-clad circuit boards. The printed circuit boards were then mounted onto a 3'' acrylic tube for support. Capacitors were placed on the two outer rings in order to create a high-pass configuration for the outer two ^{1}H

coils. These ^{1}H coils are then inductively coupled at the center of the birdcage (7). For the ^{23}Na frequency, capacitors were placed at the middle of each rung to create a low-pass configuration. This design was chosen because of its ability to provide a good amount of isolation between both frequencies while also allowing the use of low capacitances for the low-pass configuration and high capacitances for the high-pass configuration (8).

Preliminary capacitor values were calculated using the Birdcage Builder Java web app (9). Table 1 shows the input parameters for each channel and the capacitor values calculated with Birdcage Builder.

Table 1. Birdcage Builder input parameters and results.

Parameters	**^{23}Na Channel**	**^{1}H Channel**
Leg length	12.2 cm	4 cm
Trace width (endring and leg)	0.3 cm	0.3 cm
Type of leg	Rectangular	Rectangular
Type of endring	Rectangular	Rectangular
Number of legs	16	8
Configuration	Low pass	High pass
Coil radius	3.81 cm	3.81 cm
RF shield radius	5.95 cm	5.95 cm
Center frequency (at 4.7T)	52.93 MHz	200.07 MHz
Calculated capacitance	29.78 pF	16.50 pF

Bench testing

Initially, the capacitor gaps for the outer structures were left open while 30 pF (1111C Series, Passive Plus) ceramic capacitors were placed on the inner structure for tuning the ^{23}Na frequency at 52.93 MHz. The coil was placed inside an RF shield before taking any measurements. The purpose of the shield is to prevent unwanted interactions between the coil and components in the bore of the MR scanner (8). For this reason, to account for these effects, bench testing was performed with the coil inside of the shield.

Two single-loop probes were used to take an S_{21} measurement on the network analyzer (Agilent E5071C). One of the probes was placed right next to the conductor and the other one at the center of the coil. This measurement showed the resonant frequency of the inner structure of the coil. If the measured center frequency was far from the desired frequency, Equation 1 was used to find the inductance of the coil. Then, the inductance value was used to recalculate the capacitance.

$$\omega = \frac{1}{\sqrt{LC}}$$

Equation 1. Resonance Frequency

To check the resonant frequency of the ^{1}H structure at 200.07 MHz a similar procedure was followed. The capacitors from the inner structure were removed and the gaps were shorted using copper tape. Then 10pF (1111C Series, Passive Plus) capacitors were placed on the outer structures. Once both sections were tuned individually, the low-pass capacitors were placed back on the low-pass structure, and port connections and multiturn variable tuning and matching

capacitors (VMAT40HVE 1712, 1.5-40 pF range) were added to both structures, as shown in Figure 2.

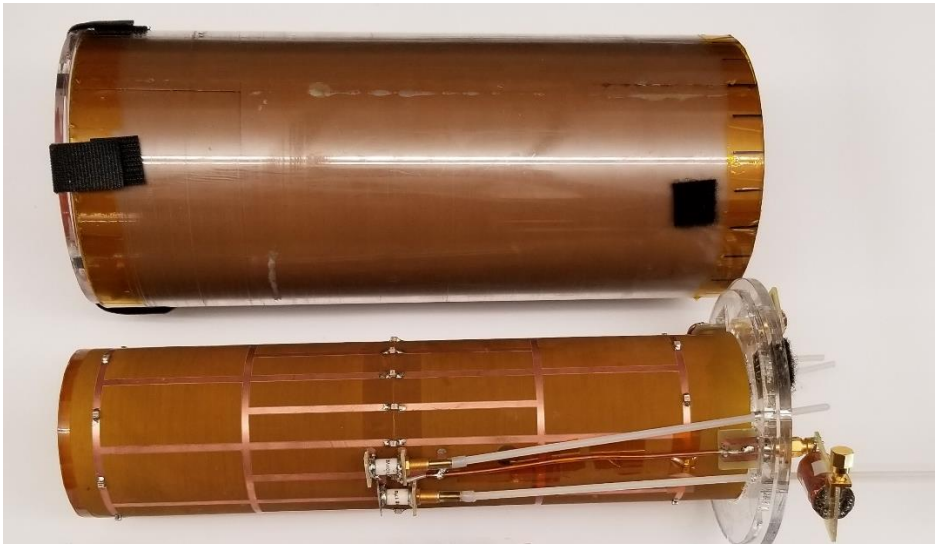

Figure 2. RF shield and birdcage coil with fixed and variable capacitors

A custom B_1 mapping system/structure was designed to make controlled and precise bench measurements using field probes. The top platform consists of a set of four rulers that allow to take measurements in the x, y, and z directions. Additionally, a set of attachments were designed to hold single or double loop probes. These attachments add an additional degree of freedom by allowing to take precise measurements at different angles. Finally, the nylon rods allow to adjust the height of the system to measure coils of different lengths. The mapping system is shown in Figure 3.

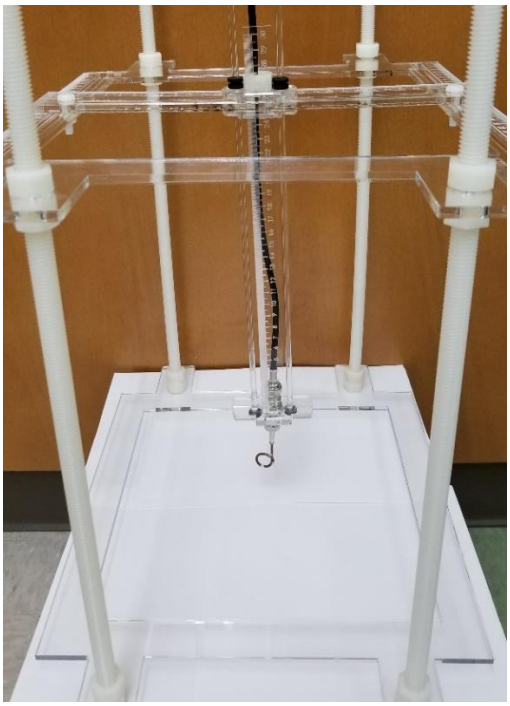

Figure 3. Custom B_1 mapping system.

To match and tune both frequencies, an S_{11} measurement was taken from both ports with all the components, including match and tune capacitors, connected on both structures. Matching and tuning was achieved at both loaded and unloaded states. The matching values obtained at both frequencies are shown in Table 2.

Table 2. S_{11} measurements of loaded and unloaded states at each frequency

State	**^{23}Na Channel**	**^{1}H channel**
Loaded	-24.4 dB	-30.1 dB
Unloaded	-27.2 dB	-27.0 dB

The S_{11} data obtained with the network analyzer was saved and plotted with MATLAB as shown in Figures 4 and 5.

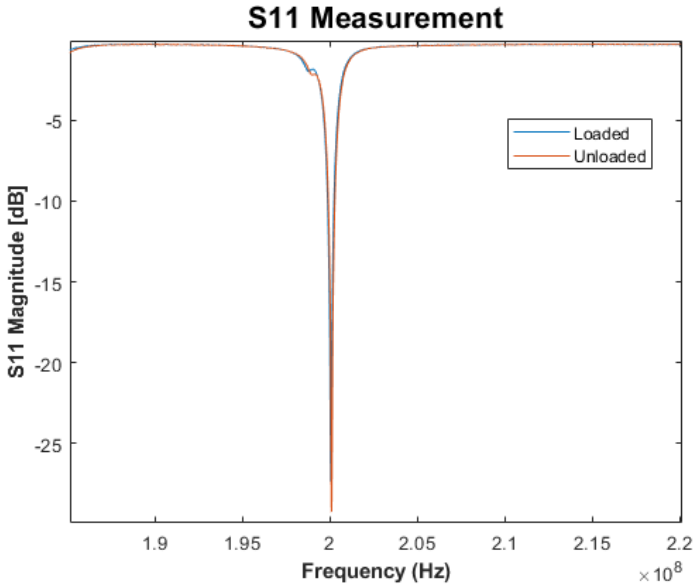

Figure 4. S_{11} measurement of unloaded and loaded ^{1}H channel.

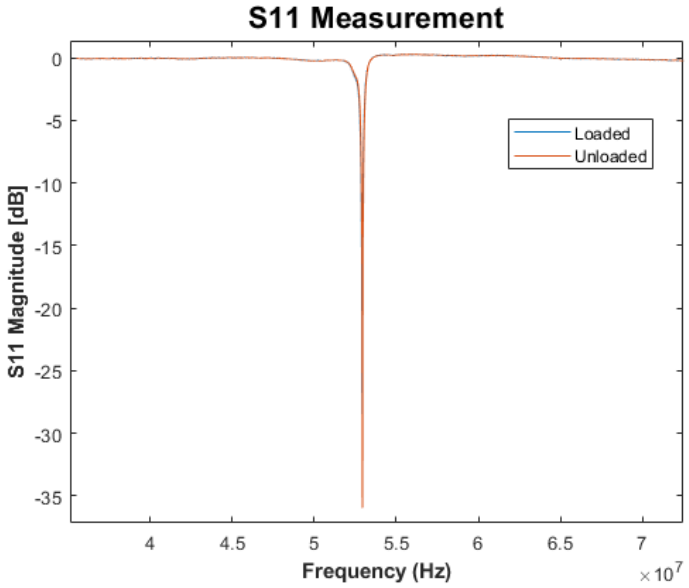

Figure 5. S_{11} measurement of unloaded and loaded ^{23}Na channel.

Once the coil was matched and tuned for both frequencies, S_{12} measurements were taken. The signal was transmitted through one of the feeding ports while the other port was connected to a 50 Ω load. The B_1 mapping system was used to place a single-loop probe at the center of the coil. It was observed that the peak representing the homogenous mode of the low-pass configuration split into two different modes due to coupling with other components and/or cables. To counteract these coupling effects, baluns tuned to their corresponding frequency were connected to each feeding port to block unbalanced currents and to reduce radiation losses within the cables (8).

To conduct bench testing, a 45 mL phantom that would mimic the loading properties of diseased tissue was created by mixing NaCl with water to achieve a concentration of 38.4 mmol/L. This value has been reported as the tissue sodium concentration level in patients with DMD (2,10). An acrylic insert was used to center the test tube, with the phantom, within the center of the birdcage coil to ensure that it is placed in the coil's most homogenous region. The insert is shown in Figure 6.

Figure 6. Acrylic insert with test tube.

The axial B_1, isolation between channels, quality factors and S-parameters of the coil were measured with the network analyzer. The homogeneity of B_1 along the length of the coil

was assessed by placing a measuring probe at the center of the coil and transmitting the signal through one of the feeding ports. The probe was shifted vertically to take S_{21} measurements at discrete positions along the center of the coil. The magnetic field of each structure was evaluated separately. The capacitors on the outer structure were removed, and the ^{1}H port was disconnected. The signal was transmitted with the coil through the ^{23}Na feeding, and the B_1 mapping system was used to place the single-loop probe at the center of the coil.

The same procedure was followed to record the axial B_1 field of the ^{1}H coil. Capacitors were placed on the outer structures and the ^{1}H port was connected. The capacitors on the inner structure were replaced with copper tape, and the ^{23}Na feeding port was disconnected. The signal was transmitted through the ^{1}H feeding port, and it was received with the single-loop probe placed inside the coil. Finally, all the components were placed back on the coil, and after tuning and matching, B_1 field measurements of both coils were taken. The magnetic field was first evaluated with the ^{1}H port transmitting the signal and the ^{23}Na port connected to a 50 Ω load, as shown in Figure 7, and then the connections were switched.

Figure 7. ^{1}H and ^{23}Na ports and baluns.

The isolation between both ports was recorded by taking an S_{12} measurement between both ports at both resonant frequencies (i.e. 52.93MHz and 200.07MHz). The loaded and unloaded quality factors (Q) were measured to evaluate losses due to sample loading when a phantom was present in the coil. Finally, S_{21} measurements were taken at 0°, 45° and 90° at the center of the coil to evaluate signal strength at both frequencies at different orientations.

Image acquisition and data processing

Additional phantoms were created by mixing NaCl and DI water in 45- and 500-mL containers to achieve sodium concentrations of 25.4 mmol/L, 38.4mmol/L, and 76.8 mmol/L. These concentrations represent healthy skeletal muscle, diseased skeletal muscle, and a higher concentration used to test the coil. A 4.7 Varian Inova Scanner was used to obtain images of the phantoms with the coil in transmit/receive mode.

A preliminary ^{23}Na image of the 45mL 76.8 mmol/L phantom was obtained to test imaging parameter values for the medium-sized phantoms. The insert shown in Figure 6 was used to place the phantom at the center of the coil.

The 500 mL 38.4 mmol/L phantom was used to obtain a proton image and to observe the homogeneity of the signal throughout the coil. The coil was placed in the RF shield, and the phantom was placed inside the coil. An acrylic piece designed to position coils in the center of the bore of the magnet was used to place the birdcage coil inside the magnet. Once this was done, the hydrogen port was connected to the signal line, and the sodium port was connected to a 50 Ω load. An ultra-low-magnetic network analyzer (AEA VIA Echo MRI) was used to ensure the coil was tuned to the right frequency and matched to 50 Ω. Then, a profile of the phantom was taken to ensure the imaging parameters used were appropriate before obtaining the image. The parameters used to obtain the multi-slice proton image are shown in Table 3.

Table 3. ^{1}H Imaging Parameters

Parameter	**Value**
Recovery time (TR)	1000 ms
Echo time (TE)	30 ms
Resolution	256x256
Number of slices	20
Slice thickness	2 mm

The scanner obtains multi-slice images in a non-sequential order to avoid a decrease in signal strength and contrast (11). Then, it creates a matrix with the k-space data in the order it was obtained.

After obtaining the multi-slice images, the connections and parameters were changed to obtain sodium images. The signal line was connected to the ^{23}Na port, and the 50 Ω load was connected to the ^{1}H port. Previous sodium MRI research has shown that image acquisition of this nucleus results in images with low spatial resolution and SNR. These issues arise as a result of the low concentration of ^{23}Na in vivo, the low gyromagnetic ratio and the short transverse relaxation times (T_2) (12-14). For this reason, several parameter values were tested to obtain a profile of the phantom with the 500mL 25.4 mmol/L phantom first. The parameters used to obtain the sodium image are shown in Table 4.

Table 4. ^{23}Na Imaging Parameters

Parameter	**Value**
Recovery time (TR)	300 ms
Echo time (TE)	6.5 ms
Resolution	64x64
Number of slices	1
Slice thickness	20 mm

After the image of this phantom was acquired, the same parameter values were used to obtain images of the other two 500 mL phantoms (i.e. 38.4 mmol/L and 76.8 mmol/L). Every time the phantom was switched, the network analyzer was used to measure the return loss of the coil, and to check the tuning and matching of the coil.

The k-space data of the proton and sodium scans was saved to be processed with a MATLAB program. The script reconstructs the image by taking the 2D Inverse Fourier Transform of the k-space data. Then, signal and noise masks are created to calculate the average of the signal and noise regions, as well as the standard deviation of the noise. After doing this, it calculates the SNR of the image and plots an SNR map with a color bar to compare different concentrations.

CHAPTER III

RESULTS

Bench testing

It was found that the axial B_1 magnitude was homogeneous at the region of interest, or the center 8 cm of the coil. The isolated B_1 measurements at each frequency are shown in Figures 8 and 9.

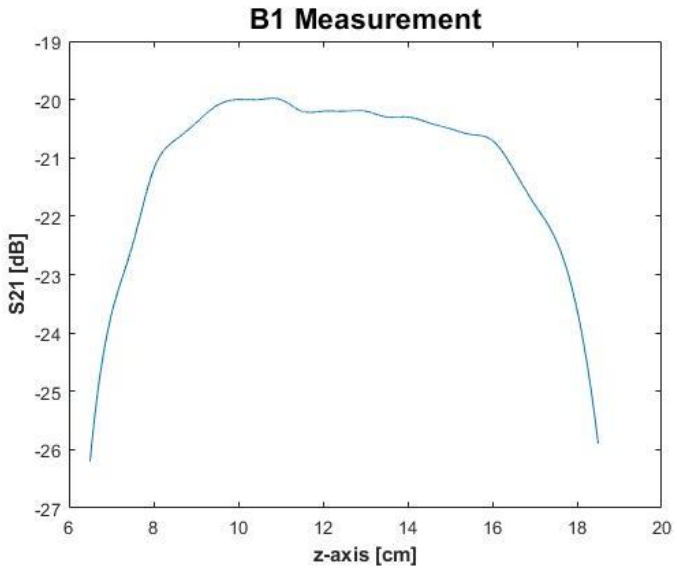

Figure 8. RF magnetic field of isolated ^{23}Na coil structure

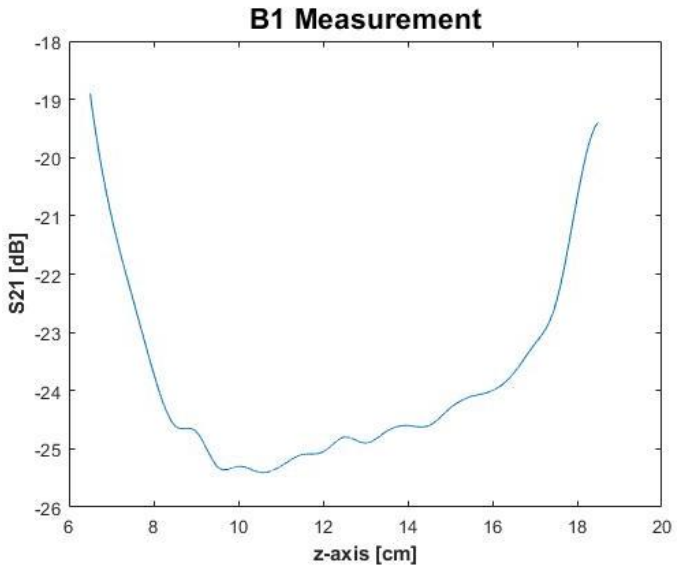

Figure 9. RF magnetic field of isolated ^{1}H coil structure

The results reported for each isolated structure are consistent with results obtained in different studies. Previous studies have reported homogeneity in the center of the inner coil structure of dual-tuned birdcage coils (15,16). In both cases, the signal strength decreased as the field probe approached the region where the end rings were located, as shown in the B_1 field measurements. This was also observed in the B_1 measurements for each channel with both coil structures in place. The results from these measurements are shown in Figures 10 and 11.

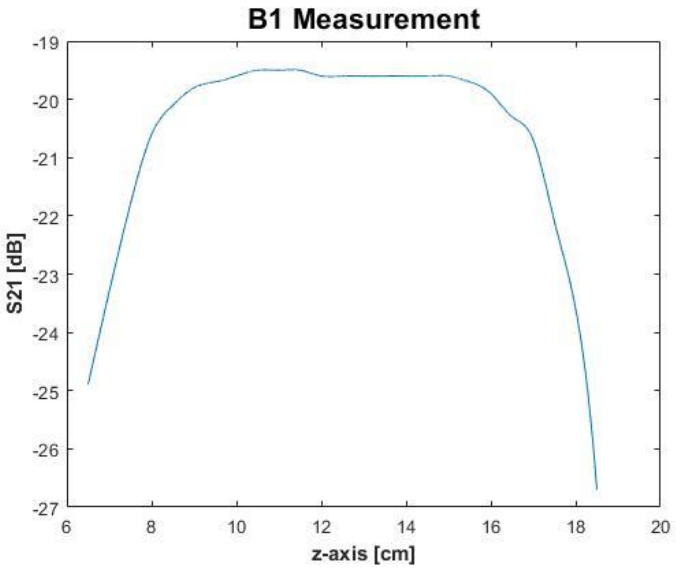

Figure 10. RF magnetic field of ^{23}Na channel

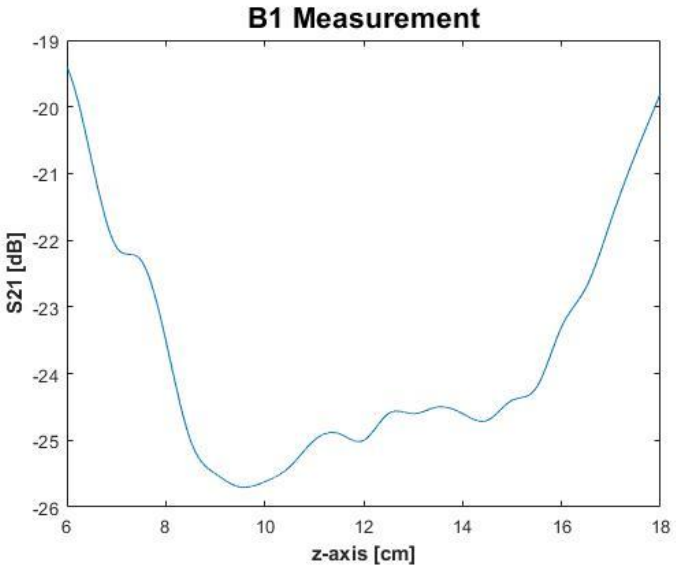

Figure 11. RF magnetic field of ^{1}H channel

The results obtained from both channels are very similar to the B_1 field measurements from the isolated structures. As shown in Figures 8 and 9, the end rings cause a decrease in signal strength, but the field is homogeneous in the center of the coil.

The S_{21} measurements taken at different angles show that the strongest signal was found at 0° for the ^{1}H channel and at 90° for the ^{23}Na channel (i.e. 0° when facing the feeding port). The values obtained at the different angles are shown in Table 5. The pick-up probe was oriented within the coil prior to taking the B_1 measurements based on the strongest signal produced for each port.

Table 5. S_{21} measurements at different orientation angles.

Orientation Angles	**^{23}Na Channel**	**^{1}H channel**
0°	-29.7 dB	-23.3 dB
45°	-23.0 dB	-27.4 dB
90°	-18.2 dB	-38.2 dB

The isolation between channels was -25 dB at 200.07 MHz and -30.9 dB at 52.93 MHz. The quality factors and the S_{11} parameters of the loaded and unloaded conditions were found using MATLAB. The Q of the loaded and unloaded ^{1}H channel were 351.1 and 359.9, respectively. The Q of the loaded and unloaded ^{23}Na channel were 293.9 and 300.7, respectively. These Q values indicate good overall coil performance (17). However, the small change between loaded and unloaded Q values indicate that the primary resistive losses can be attributed to the coil and not to loading.

Image acquisition and data processing

The multi-slice proton images were acquired with a Varian scanner. The scanner acquired the slice images in a non-sequential order. However, they were arranged to represent a sequential order, as shown in Figure 12.

The distortions present in some of the slice images can be attributed to imaging outside the linear region of the gradients. The most homogeneous region of the coil corresponds to the inner 8 cm of the coil, as shown in slices 7, 8, 16, and 17. The slices located outside this range correspond to the regions located outside of the inner coil structure, the linear gradient region, and the phantom region. The slice with the highest SNR value (57.4) was slice 17, and the average SNR of the inner 10 cm of the coil varied by ± 3.8.

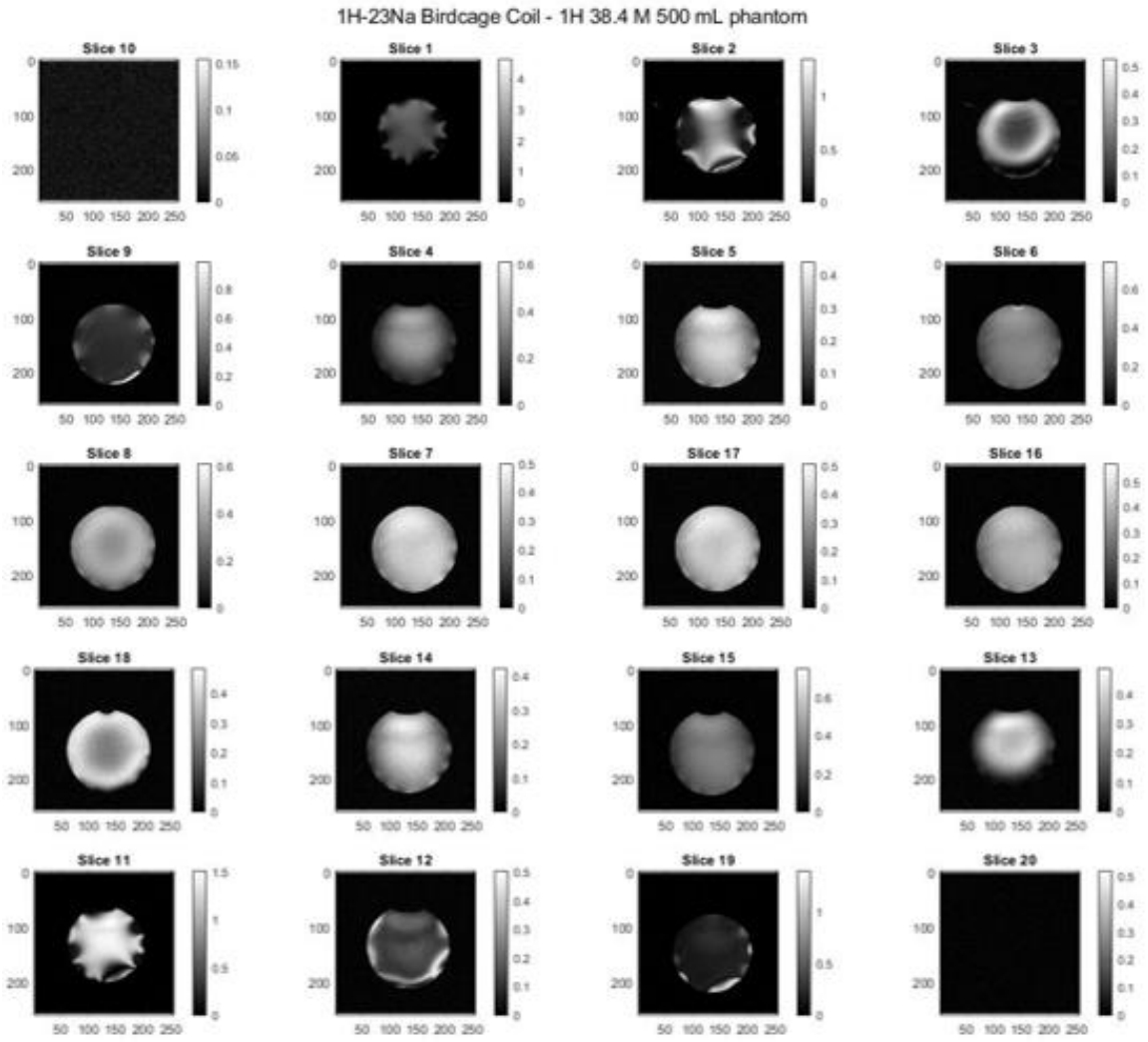

Figure 12. Multi-slice Proton Images

The sodium images of the 45-mL and 500-mL phantoms with concentrations of 38.4 mmol/L and 76.8 mmol/L are shown in Figures 13, 14 and 15. Additionally, the SNR maps of the 500 mL phantom images are shown in Figures 16 and 17. The average SNR of the 500 mL 38.4 mmol/L phantom was 3.76, and the average SNR of the 500 mL 76.8 mmol/L phantom was 4.72.

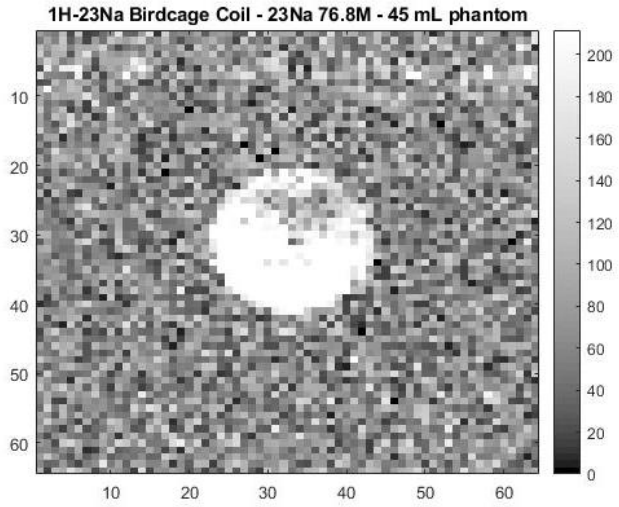

Figure 13. ^{23}Na image of 45 mL phantom with 76.8 mmol/L concentration

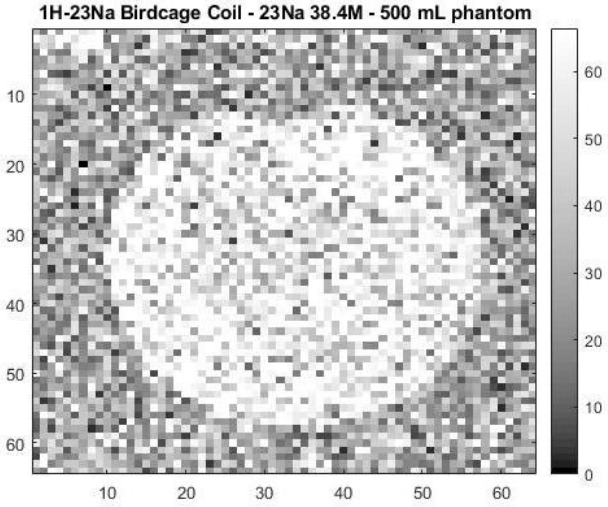

Figure 14. ^{23}Na image of 500 mL phantom with 38.4 mmol/L concentration

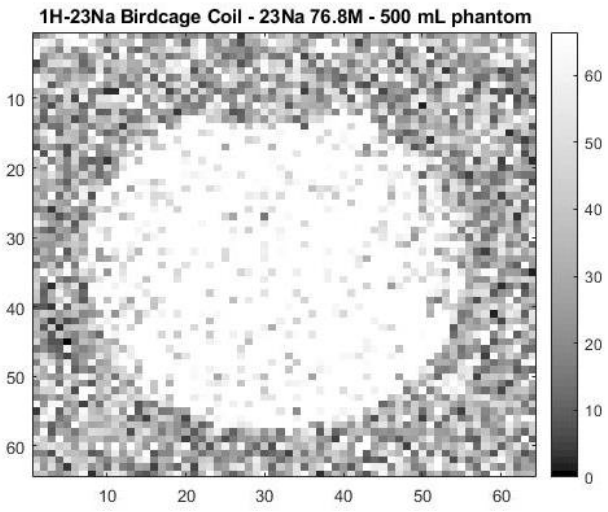

Figure 15. ^{23}Na image of 500 mL phantom with 76.8 mmol/L concentration

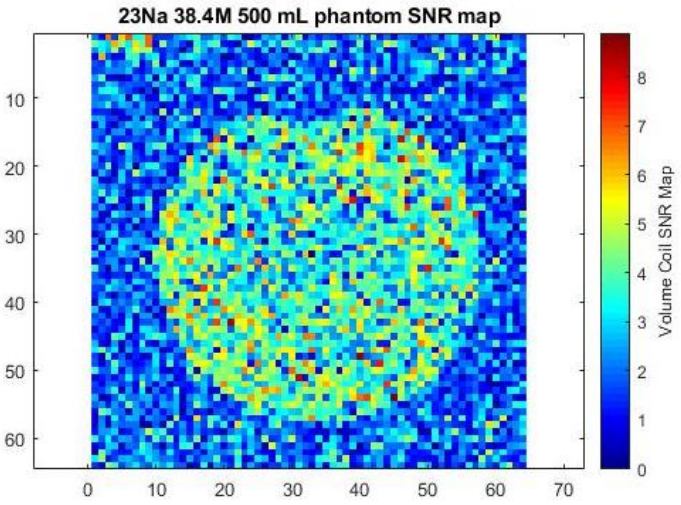

Figure 16. SNR map of phantom with 38.4 mmol/L concentration

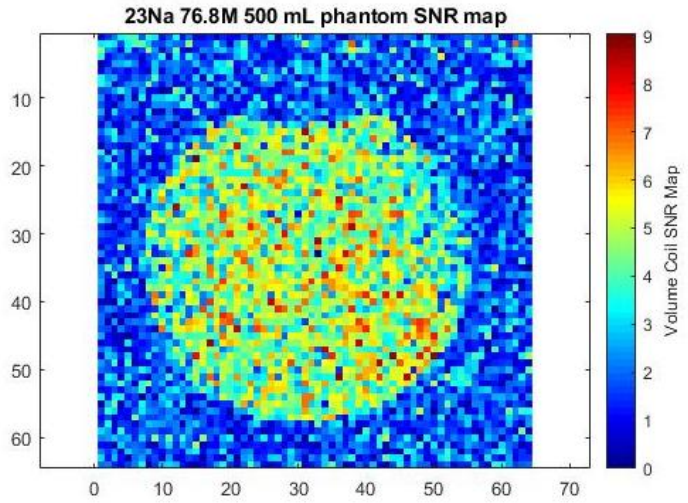

Figure 17. SNR map of phantom with 76.8 mmol/L concentration

The SNR maps of the images show a higher SNR for the higher concentration phantom, as expected. The average values of the signal and noise regions are shown in Table 6.

Table 6. Signal and Noise Average Values

	38.4 mmol/L phantom	**76.8 mmol/L phantom**	**Percentage difference**
Signal average	60.2	86.7	36.1 %
Noise average	30.4	32.8	7.49 %
Average SNR	3.76	4.73	22.7 %

The results shown in Table 6 suggest that even though there was a slight increase in noise average, the increase in signal was more significant. However, additional phantoms are needed to determine if there is a linear relationship between increasing concentration values and their corresponding signal-to-noise ratios.

CHAPTER IV

CONCLUSION

Magnetic resonance imaging is a non-invasive imaging technique widely used to study and diagnose many diseases and conditions. Proton (^{1}H) is the NMR active nuclei most commonly used for MR imaging due to its natural abundance in the body. However, additional biochemical information can be obtained from other NMR active nuclei in the body, such as sodium (12).

Sodium MRI could provide relevant information for the study of DMD. However, it represents a challenge due to the specialized pulse sequence and reconstruction techniques required to image this nucleus with a high SNR. Additionally, custom hardware must be developed to meet the needs and requirements of every application. More work needs to be done to address the lack of information regarding the impact abnormal sodium concentration levels have in muscle degeneration. For this reason, the linear dual-tuned birdcage coil designed and constructed for this project is relevant to the study of DMD. Evaluating diseased tissue from GRMD models could provide meaningful information about treatment efficacy and disease progression, and this project represents a step towards that end.

The results of the bench measurements show that the birdcage coil is suitable for this application. The B_1 field is homogeneous for ^{23}Na and ^{1}H over the region of interest. Furthermore, the images obtained with the 500 mL saline solution phantoms demonstrate the ability to distinguish between different sodium concentration levels.

Future work will include improved coil designs to decrease resistive losses. Implementing a quadrature design would help increase SNR and reduce RF power during

transmission (18). Imaging phantoms that mimic the size of the tissue samples (i.e. 45 mL phantoms) will eliminate the distortions caused by non-linearities in the gradient coil. Moreover, data obtained from imaging phantoms with a wider range of concentrations will allow curve fitting analysis to determine the relationship between sodium concentration and SNR. In addition, gel phantoms that mimic concentration levels in tissue and its relaxation properties will allow to further test the coil's ability to image tissue. Imaging parameters used for testing will help establish the parameters needed to image harvested tissue from GRMD models.

REFERENCES

1. Joe N. Kornegay SMT, Doris M. Miller, Donald C. Levesque. Muscular dystrophy in a litter of golden retriever dog. Muscle Nerve 1988;11(10).

2. M.-A. Weber AMN, K. Jurkat-Rott, F. Lehmann-Horn. Sodium (^{23}Na) MRI detects elevated muscular sodium concentration in Duchenne muscular dystrophy. Neurology 2011;77(23).

3. Carole Hirn GS, Olivier Petermann, Emmanuelle Roulet, Urs T. Ruegg. Nav1.4 Deregulation in Dystrophic Skeletal Muscle Leads to Na+ Overload and Enhanced Cell Death. Journal of General Physiology 2008;132(2):199-208.

4. Barry J. Cooper NJW, Hansell Stedman, Beth A. Valentine, et al. The homologue of the Duchenne locus is defective in X-linked muscular dystrophy of dogs. Nature 1988;334(6178):154-156.

5. Claire Wary TN, Jean-Laurent Thibaud, Aurélien Monnet, et alr. Splitting of Pi and other ^{31}P NMR anomalies of skeletal muscle metabolites in canine muscular dystrophy. NMR in Biomedicine 2012;25(10):1160-1169.

6. Dennis Klomp WK, Hans Hoogduin, Alexander Raaijmakers, et al. Practical design of RF transmit and receive arrays. . 2011; Leipzig. p 6.

7. J. Murphy-Boesch RS, L. Carvajal, TR. Brown. Two configurations of the four-ring birdcage coil for ^{1}H imaging and ^{1}H-decoupled ^{31}P spectroscopy of the human head. Journal of Magnetic Resonance B 1994;103(2):103-114.

8. RF Coils for MRI2012.

9. C. L. Chin CMC, S. Li, B .J. Dardzinski, M. B. Smith. BirdcageBuilder: Design of Specified-Geometry Birdcage Coils with Desired Current Pattern and Resonant Frequency. Concepts in magnetic resonance 2002;15(2):156-163.

10. M.-A. Weber AMN, M. B. Wolf, K. Jurkat-Rott, et al. Permanent muscular sodium overload and persistent muscle edema in Duchenne muscular dystrophy: a possible contributor of progressive muscle degeneration. Neurology 2012;259(11):2385-2392.

11. J. Bruce Kneeland AS, Felix W. Wehrli. Effect of Intersection Spacing on MR Image Contrast and Study Time. Radiology 1986;158:819-822.

12. Neal K. Bangerter GJT, Meredith D. Taylor, Joshua D. Kaggie. Quantitative sodium magnetic resonance imaging of cartilage, muscle, and tendon. Quantitative Imaging in Medicine and Surgery 2016;6(6):699-714.

13. Bottomley PA. Sodium MRI in Man: Technique and Findings. eMagRes 2012;1:353-366.

14. Guillaume Madelin J-SL, Ravinder R. Regatte, Alexej Jerschow. Sodium MRI: Methods and applications. Progress in Nuclear Magnetic Resonance Spectroscopy 2014;79:14-47.

15. Potter WM. Radiofrequency Coil Design and Application to Magnetic Resonance Imaging and Control of Micro-beads. Athens, Georgia: The University of Georgia; 2005. 75.

16. Yunsuo Duan BSP, Feng Liu, Truman R. Brown, Tamer S. Ibrahim, and Alayar Kangarlu. Computational and Experimental Optimization of a Double-Tuned 1H/31P Four-Ring Birdcage Head Coil for MRS at 3T. Journal of Magnetic Resonance Imaging 2009;29:13-22.

17. Giulio Giovannetti RF, Luigi Landini, et al. Conductor Geometry and Capacitor Quality for Performance Optimization of Low-Frequency Birdcage Coils. Journal of Magnetic Resonance B 2004;20B(1):9-16.

18. G. H. Glover CEH, N. J. Pelc, et al. Comparison of Linear and Circular Polarization for Magnetic Resonance Imaging Journal of Magnetic Resonance 1985;64:255-270.